PERGAMON

International Journal of Solids and Structures 38 (2001) 7747–7768

INTERNATIONAL JOURNAL OF SOLIDS and STRUCTURES

www.elsevier.com/locate/ijsolstr

Fracture mechanisms induced in a brittle material by a hard cutting indenter

Bernardino Chiaia *

Department of Structural and Geotechnical Engineering, Politecnico di Torino, Corso Duca degli Abruzzi 24, 10129 Torino, Italy

Received 14 November 2000

Abstract

The process of indentation of brittle and quasi-brittle materials has been extensively investigated both from the experimental and the theoretical point of view. Also, the elastic stress fields induced by sliding bodies are well known and have been used to predict fracture patterns below moving contacts. Quite surprisingly, only a few studies have tried to explain the mechanics of cutting due to an indenter which penetrates inside the material. In this paper, an attempt is made to find some general relations for the cutting process in quasi-brittle materials, under different hypotheses for the microscopic failure behaviour, namely a simple frictional mechanism, plastic crushing and linear elastic fracture mechanics. These mechanisms interact with each other, and provide a particular load-penetration law and a peculiar cutting advancement. Some numerical simulations by the lattice model have been also carried out, in order to verify the assumptions. Dimensional analysis permits to highlight remarkable size-scale effects on the cutting strength and provides some hints for enhancing the performances of cutting tools.

Keywords: Indentation; Cutting; Size effects; Heterogeneous materials

1. Introduction

Many technological operations involve two or more contacting bodies sliding with respect to one another. A series of damage mechanisms can occur in these situations, for instance fretting fatigue and wear. Incommensurable economic losses can be ascribed to these phenomena. In a totally different context, scratching and cutting represent fundamental manufacturing processes, as in the case of cutting precious and ornamental stones and of rock excavations and drilling. Therefore, the mechanics of these processes has been an important object of research since many years.

In the framework of plasticity, the *slip-lines theory* was developed to explain the collapse mechanisms of ductile materials under various kinds of loading (Hill, 1950). The starting assumptions are those of rigid – perfectly plastic material and of plane strain conditions. Looking for conditions of simple shear deformation, the slip lines can be found by geometrical considerations, also taking into account friction between

* Tel.: +39-11-564-4866; fax: +39-11-564-4899.
E-mail address: chiaia@polito.it (B. Chiaia).

0020-7683/01/$ - see front matter
PII: S0020-7683(01)00117-2

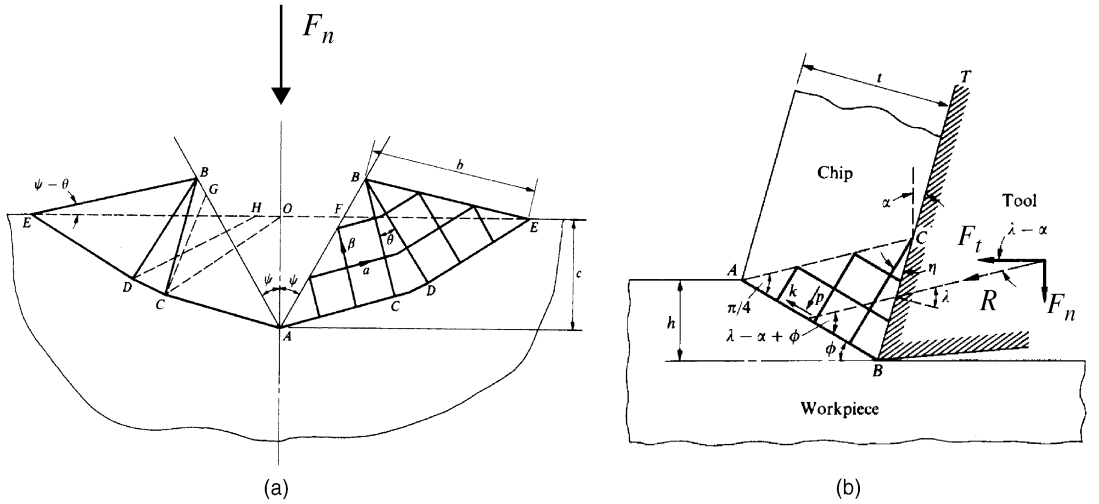

Fig. 1. Slip-lines field obtained (a) in the case of plastic indentation due to a rigid wedge, and (b) in the case of plastic cutting with positive rake angle (Hill, 1950).

the cutting tool and the material. In Fig. 1a, the plastic flow of a ductile material subjected to indentation is shown. The load-penetration law is different from the linear elastic one (which is parabolic, see Section 2), because the material is more compliant. The plastic cutting mechanism (*continuous chipping*) is depicted in Fig. 1b. Compressive stresses on the shear plane must be high enough to allow the material to undergo considerable shearing strains without fracture. This depends on the normal component of the force and on the rake angle α. Only in this way it is possible to develop the continuous chip commonly detected by the experiments (see Fig. 2). In the absence of cutting fluids, and especially at low speeds, discontinuous chipping may occur, even in mild steels, due to friction between tool and chip (Merchant, 1944).

The process of indentation is completely different in the case of brittle materials (Lawn and Wilshaw, 1975) and depends also on the shape of the indenter. When brittle materials are loaded by an indenter, three different zones can be distinguished into the material (Fig. 3). Immediately below the wedge, an *hydrostatic*

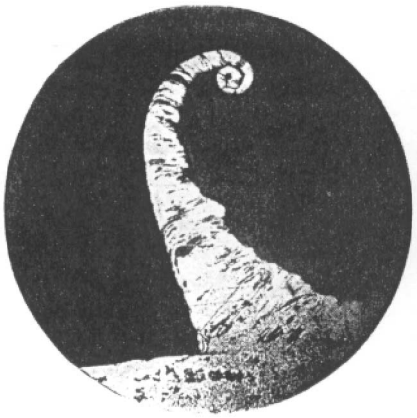

Fig. 2. Experimentally detected continuous chipping in ductile steels (Merchant, 1944).

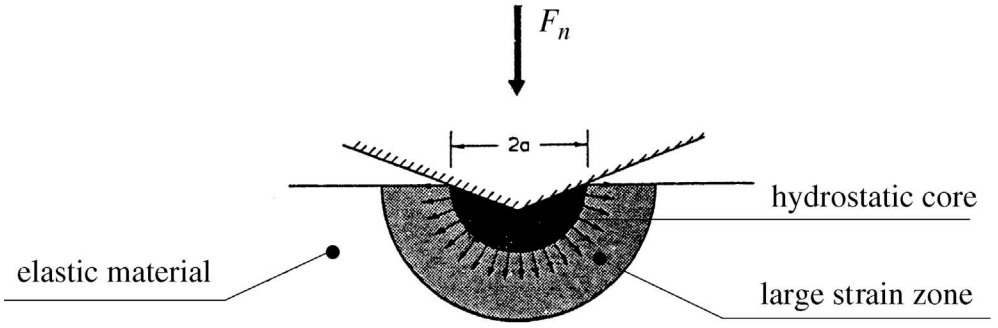

Fig. 3. Indentation of brittle materials: formation of the hydrostatic core and of the large-strain zone.

core develops, which is due to the high triaxial compressive stresses induced beneath the indenter. This zone may collapse only by *crushing* and *fragmentation* mechanisms, resembling the effects of strong impacts or explosions. Outside the compressed core, a surrounding zone of large strains develops due to the pushing action of the core. In this area, *tensile cracks* may be initiated starting from pre-existing flaws in the material. Outside this large area (whose size depends on the contact area, on the friction between wedge and base material and on the normal load F_n), the material behaves elastically, and the stress fields predicted by the linear theories can be considered valid.

Fracture patterns in brittle materials, under *blunt indenters*, usually start as ring surface cracks immediately outside the contact area. By increasing the normal load, these surface cracks evolve into the so-called *Hertzian cone cracks* ($\vartheta = 30°$–$40°$), experimentally revealed by a multitude of tests on glass and other brittle materials (Fig. 4a). The laws of propagation of the Hertzian cracks were analysed by Roesler (1955) in the framework of linear elastic fracture mechanics (LEFM). He demonstrated that the phenomenon is *stable*, i.e., an increase of the load is always required to propagate the crack. The energy release rate was found to be like:

$$G_I \sim \frac{F_n^2}{ER^3}, \tag{1}$$

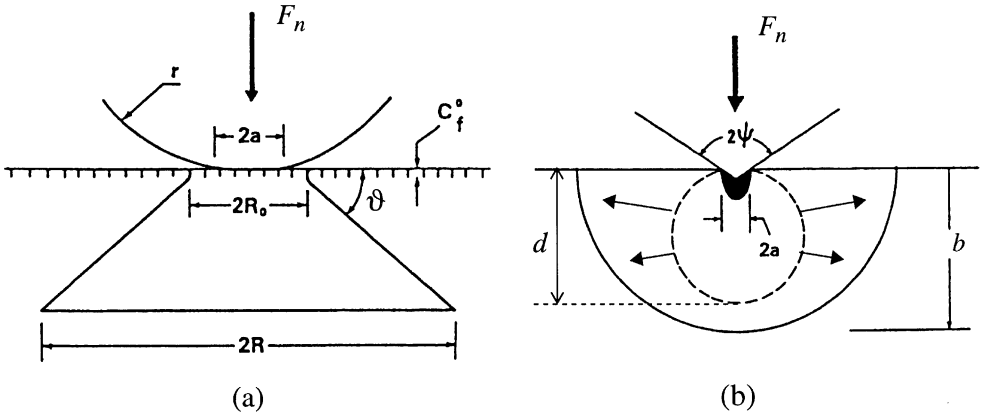

Fig. 4. Indentation fracture in brittle materials: (a) Hertzian cone cracks under blunt indenters, and (b) transition from splitting penny-shaped cracks to median-vent cracks under sharp indenters.

where E is the elastic modulus of the material. Thus, the radius R of the cone scales with the normal load F_n according to: $R \sim F_n^{2/3}$. This relation between the extent of damage and the indentation force has been verified in many situations. Roesler (1955) showed also that the above result does not contradict the empirical Auerbach's law, which states that the fracture load F_u is proportional to the radius of the punching sphere.

In the presence of *sharp indenters* (e.g. cones or pyramids), the high hydrostatic stresses beneath the tip provide different fracture patterns (Lawn and Swain, 1975). The splitting action of the confined core results in the propagation of an embedded *penny-shaped crack* below the indenter, whose size is controlled by the size of the hydrostatic core. By increasing the load, the penny cracks evolve into the *half-penny* configuration, where the crack reaches the surface (Fig. 4b). This was called the *median-vent* crack propagation. The energy release rate, in this case, can be written as:

$$G_I \sim \frac{H}{E}\frac{F_n}{d}, \tag{2}$$

where H is the hardness number of the material and d is the diameter of the penny-shaped crack.

Besides the basic patterns described before, other shapes of cracks may develop under indentation. Their occurrence depends on the loading rate, on the density of pre-existing flaws and on the presence of weak planes in the material microstructure. Thus, the real situations if often much more complex than the theory. For instance, it has been experimentally shown that there is always a transition from "blunt" to "sharp" modes of fracture with increasing the load, due to the progressive development of the hydrostatic core (see Fig. 5). Cook and Pharr (1990) made an extensive experimental campaign on brittle materials obtaining a

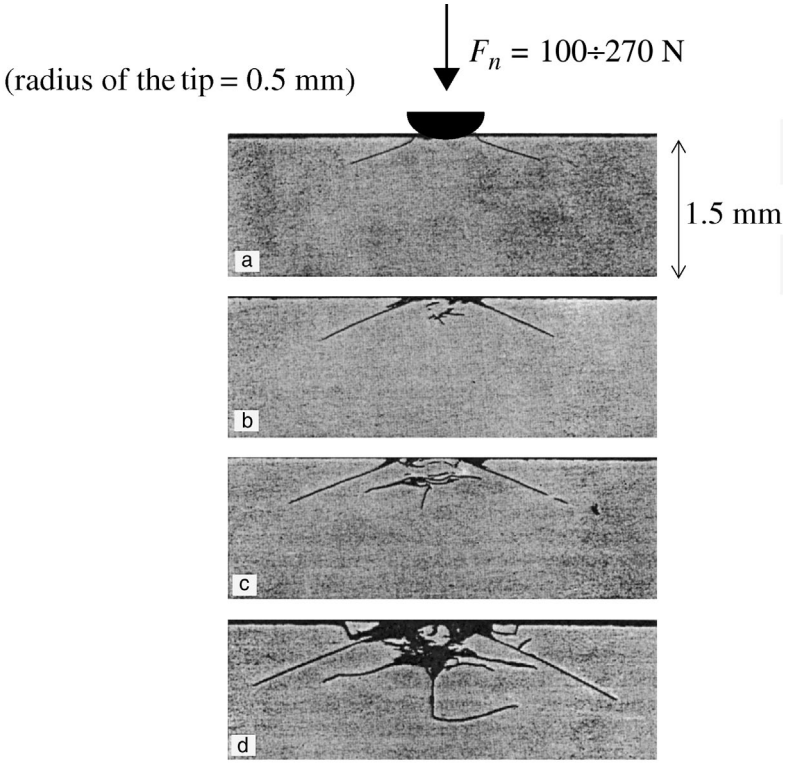

Fig. 5. Experimental crack patterns in soda-lime glass under a blunt rigid indenter (Lawn and Wilshaw, 1975). Notice the transition from Hertzian cones to median splitting cracks as the load is increased.

wide variability of crack patterns, depending on the different boundary conditions. As an example, radial cracks often develop under high strain rates (e.g. under impact or percussive drilling), or may be induced by the particular shape of the indenter, as for example by a pyramidal wedge. Lateral cracks are likely to occur under the combined action of horizontal and vertical forces, and may lead to extensive chipping and spalling ahead of the indenter.

The effects of material heterogeneity can be very important in the case of the so-called *quasi-brittle materials* (like concrete and many natural rocks). The role of microstructural disorder is essential because it provides a certain amount of 'ductility'. Moreover, these materials show considerable size effects in the mechanical response, and thus require an ad hoc modelization of the fracture processes.

Cook et al. (1984) studied the process of crack growth in a hard rock (granite) loaded by a flat rigid indenter. The experiments showed that a randomly diffused microcracking stage develops beneath the indenter, superimposed to the cone patterns detected in brittle materials (Fig. 6a). The load-penetration curve is approximately linear until a certain point A (Fig. 6b). In the first three stages, in fact, a small number of microruptures occur, as testified by the practical absence of acoustic emission events. Instead, in the IV stage, there is a sudden increase of emission counts and the curve becomes nonlinear. Finally, after the peak load, a burst of microcracking events occurs. The *softening* regime comes into play, characterized by a negative slope in the load-penetration diagram.

This peculiar mechanical behaviour implies that the material can dissipate a considerable amount of energy after the peak load. The energy is consumed in the so-called *fracture process zone*, which is a wide zone around the main crack tips, where diffused damage comes into play. The extent of the process zone depends on the material microstructure and also on the size of the indenter. The presence of characteristics lengths of damage in each material imply the occurrence of size effects, often revealed when dealing with quasi-brittle materials like concrete and rocks (Carpinteri, 1989). In Fig. 7, two different kinds of size effects are reported. In Fig. 7a, the normalized peak stress (indentation strength) is shown to decrease as the diameter of the punch increases. The material's resistance to the indentation of large punches shows a decrement of about 20% compared to small punches. This means that the fracturing and chipping processes, for a given material, become more efficient as the size of the indenter increases. In Fig. 7b, another kind of size effect is depicted, namely the (normalized) measured elastic modulus is larger as the diameter of the indenter increases. This effect is important when the load-penetration law for a certain cutting tool

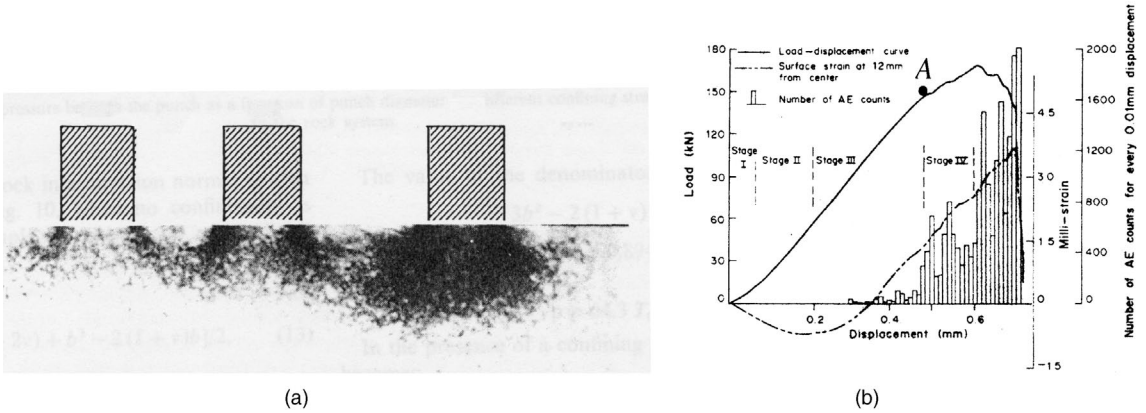

Fig. 6. Indentation experiments on quasi-brittle rocks performed by Cook et al. (1984): (a) diffused microcracking with increasing load; (b) load-penetration response with corresponding acoustic emissions records.

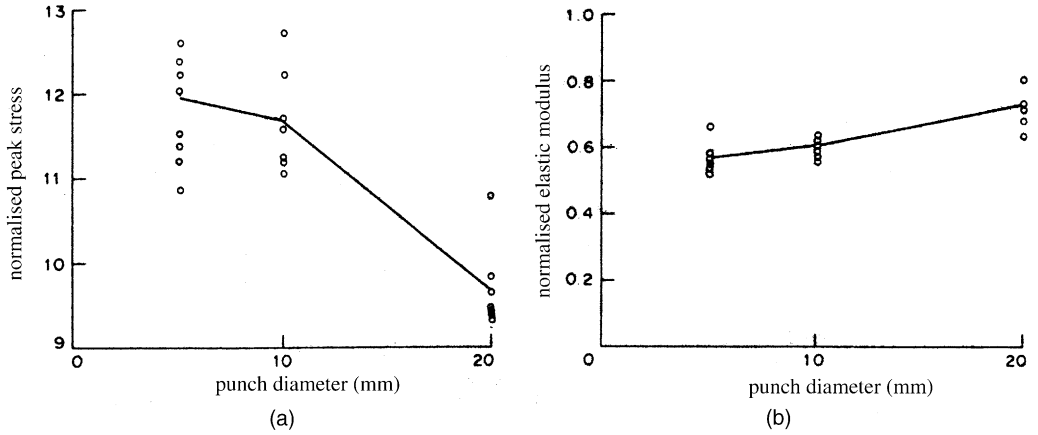

Fig. 7. Size effects in the indentation process (Cook et al., 1984): decrease of the indentation strength (mean peak pressure normalized with respect to the uniaxial compressive strength) (a) and increase of the elastic modulus (normalized with respect to Young's modulus measured by triaxial tests) (b), as the diameter of the punch increases.

(e.g. a small diamond) is to be predicted, because the moduli measured at large scales (e.g. standard laboratory tests) may considerably differ from the values valid at the microscale.

Contrarily to the process occurring in ductile materials (Fig. 1b), the process of cutting brittle and quasi-brittle materials is a stepwise phenomenon, because chip formation is discontinuous. The penetration of the indenter is, of course, a necessary condition, but the mechanisms of material removal are totally different from those of simple indentation. Positive rake angles induce tensile stresses inside the base material. Therefore, primary chipping arises mainly from fracture propagation driven by tensile stresses (Mode I and Mode II propagation). Instead, when the rake angle is negative, which is most often the case (also owing to wearing of the indenters), compressive stresses prevail ahead of the tool, and fracture cannot propagate in Mode I in front of the indenter. In this case, *crushing* is certainly the first mechanism of energy dissipation, and internal friction becomes crucial.

In Fig. 8, an experimental diagram of the cutting force versus the tool advancement is shown (Lopez Jimeno et al., 1995). According to the diagram, the cutting process can be divided into two different stages. The first is a stress-growing stage, with fine fragmentation (pulverization) immediately ahead of the wedge and stable crack growth in the base material. In this stage, a considerable amount of elastic energy is accumulated. The second stage corresponds to the so-called *primary chipping*, characterized by the separation and removal of a large fragment. The peaks of the cutting force correspond to major chips formation and their value is practically constant.

The crack patterns produced by a hard sphere scratching the surface of a soda-lime glass are shown in Fig. 9 (Lawn and Wilshaw, 1975). Notice the stepwise chipping formation along chevron-like patterns, clearly visible inside the main groove. The lateral size of the chips is practically constant, in perfect agreement with the constant peak value of the cutting force (Fig. 8). This also implies a direct proportionality between the size of the indenter and the size of the groove.

In the following, after a brief review of the elastic solutions of rigid indentation, the assessment of a reliable load-penetration law for quasi-brittle materials is pursued, with the help of numerical lattice simulations. Afterwards, the relations between the cutting force and the normal force are discussed by considering three different mechanisms of energy dissipation and material removal. Dimensional analysis will permit to evidence remarkable size effects on the specific cutting energy, which are of considerable interest for microcutting and drilling operations.

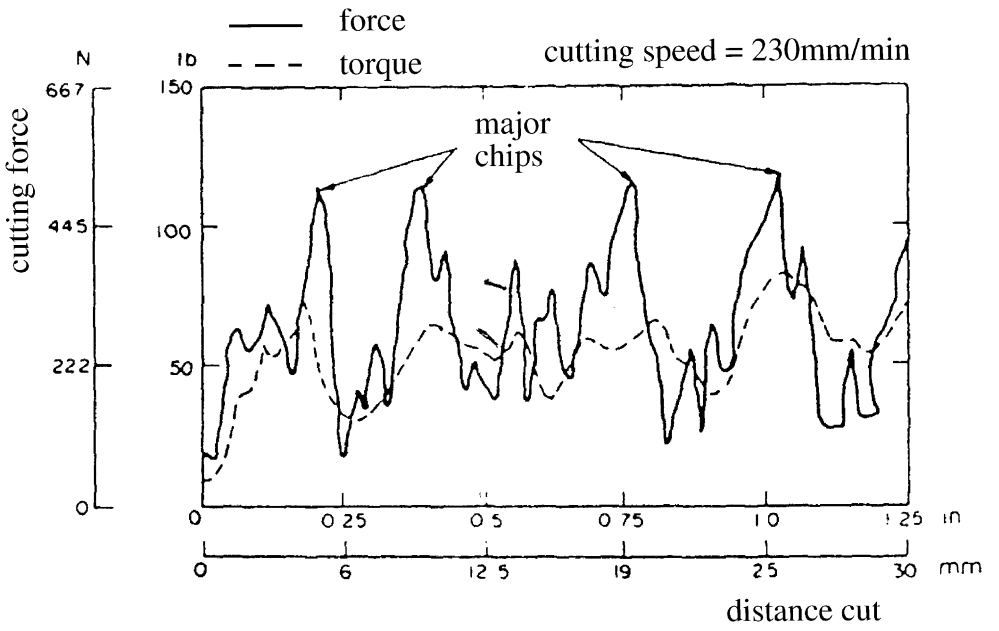

Fig. 8. Experimental diagram of the cutting force as a function of the distance cut (cutting of sandstone, by Lopez Jimeno et al. (1995)).

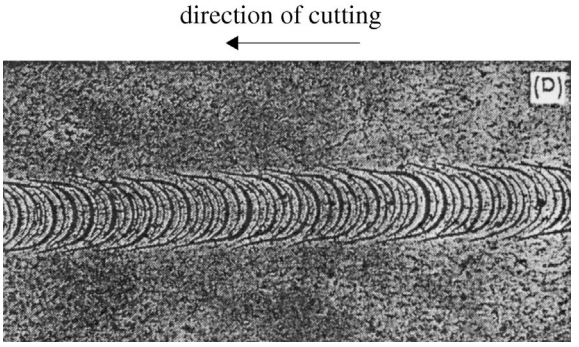

Fig. 9. Experimental crack patterns produced by a tungsten carbide sphere sliding over a soda-lime glass specimen (Lawn and Wilshaw, 1975).

2. Load-penetration laws and elastic stress fields below rigid indenters

The normal force-penetration law is the fundamental parameter controlling the cutting process. The cutting force depends on the depth of indentation, and the stress field created by indentation helps fracturing and removing the base material. Thereby, a reliable model for penetration is of major importance. The starting point is represented by the solutions obtained for the indentation of an elastic half-space by a rigid indenter (Johnson, 1985; Barber, 1992; Hills et al., 1993). Although the real phenomenon involves plasticity, damage and fracture, the elastic solutions are meaningful because they represent an *energy bound* for all other constitutive behaviours. It is interesting, in this context, to recall three basic situations, namely the spherical punch (blunt indenter), the flat punch, and the sharp conical indenter (Fig. 10).

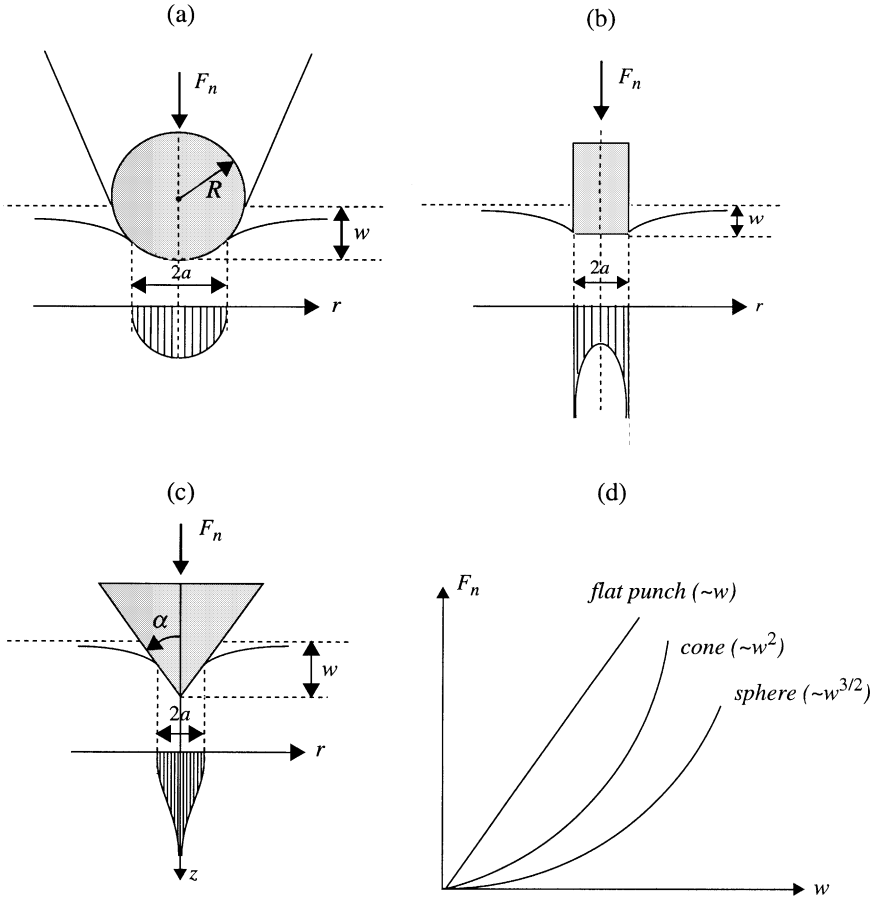

Fig. 10. Basic schemes of elastic indentation with corresponding pressure distributions: (a) blunt rigid sphere, (b) flat punch, (c) circular cone, and (d) theoretical form of the load-penetration laws.

In the case of the spherical punch, the problem is axisymmetrical and inherently nonlinear. The problem is governed by a characteristic length, i.e., the radius R of the sphere (see Fig. 10a). The well-known solution is due to Hertz (1882), and provides the following relations: $a \sim F_{\mathrm{n}}^{1/3}$, $A_{\mathrm{c}} \sim F_{\mathrm{n}}^{2/3}$, $w \sim a^2/R$, where a is the radius and A_{c} the area of the circular contact domain, F_{n} is the normal load and w is the penetration of the indenter starting from the undeformed state. Combining the previous relations, it is easy to obtain the following nonlinear form of the penetration law:

$$F_{\mathrm{n}} \sim w^{3/2}. \tag{3}$$

In terms of any radial coordinate r, the nonsingular pressure distribution can be expressed as follows (i.e., as a function of the radius of contact a):

$$p(r) = \frac{4G\sqrt{a^2 - r^2}}{\pi(1-\nu)R}, \tag{4}$$

where G is the shear modulus of the base material. The maximum value of the pressure, exactly below the axis of symmetry, is equal to:

$$p_{\max} = \frac{3}{2}\frac{F_n}{\pi a^2}. \tag{5}$$

In the case of the rigid flat punch, the problem is axisymmetrical and linear, since the area of contact is constant ($A_c = \pi a^2$). The radius a of the contact area represents the characteristic length of the problem (see Fig. 10b). In terms of any radial coordinate r, the singular pressure distribution (Barber, 1992), can be expressed as follows:

$$p(r) = \frac{F_n}{2\pi a\sqrt{a^2 - r^2}}. \tag{6}$$

The pressure becomes infinite at the edge of the punch. It is interesting to note that there is a square-root singularity, i.e., the same singularity of LEFM. This circumstance permits to treat crack initiation below the punch naturally. The load-penetration law is linear, as one could expect from dimensional analysis, and can be written as:

$$F_n = \frac{4Ga}{(1-\nu)}w. \tag{7}$$

The problem of a cone indenting an elastic half-space is sketched in Fig. 10c. Contrarily to the previous cases, this is a self-similar problem because no characteristic length is present. If w is the tip penetration, F_n is the normal force, α the semi-angle of the indenter, E Young's modulus of the half-space and ν its Poisson ratio, a straightforward application of dimensional analysis provides:

$$\frac{F_n}{Ew^2} = \Psi(\alpha, \nu), \tag{8}$$

where Ψ is a function independent of F_n, E, w. This relation defines the quadratic dependence of the normal load on the penetration. It does not depend on the shape of the punch cross-section, provided it is a circle or a regular polygon. In the case of the circular cone, the exact solution of the problem was determined in closed form by Love (1939) and Sneddon (1965), and is given by:

$$\frac{F_n}{Ew^2} = \frac{\tan\alpha}{\pi(1-\nu^2)} = K_0\Phi(\alpha, \nu), \tag{9}$$

where a shape factor $K_0 = 2/\pi$ has been introduced and Φ is a particular non-dimensional function. Generalizing for a n-sided regular pyramid, one can write:

$$\frac{F_n}{Ew^2} = K_n\frac{2\tan\alpha}{(1-\nu^2)} = K_n\Phi(\alpha, \nu). \tag{10}$$

The shape factor K_n can be computed for wedges of arbitrary shapes, starting from the conical one, noting that the ratio between the normal forces, at the same penetration w, is given by $K_n/K_0 = F_n/F_0$ (Borri-Brunetto, 2000). In the case of the circular cone, the solution for the pressure distribution in the contact area is:

$$p(r) = \frac{E\cot(\alpha)}{\pi(1-\nu^2)}\cos\,\mathrm{h}^{-1}\left(\frac{a}{r}\right). \tag{11}$$

A logarithmic singularity, independent of the wedge angle, is therefore present at the tip. In the plane orthogonal to the cone axis z, an infinite hydrostatic field is present. Instead, below the tip, the maximum shear stress is finite and its value (which increases with sharpness) is given by:

$$(\tau_{zr})^{\max} = \frac{E}{2(1-\nu^2)}\cot(\alpha). \tag{12}$$

In this case, contrarily to the spherical indenter, yielding occurs immediately below the tip and not inside the material. This explains why common hardness measurements on materials are performed by means of sharp indenters.

The three qualitative load-penetration laws are shown in Fig. 10d. The linear relation valid for the flat punch represents a limit situation, while both the other geometries provide an *upward concavity*. One should keep in mind that the above solutions were obtained under the hypothesis of rigid indenter, and should be modified if the elastic deformations of the indenter become significant. However, in the case of the common cutting tools used for concrete and rocks, these effects are negligible.

From the pressure distribution acting on the contact area, the elastic stress field inside the material can be calculated. When the rigid punch is assumed to slide over the half-space, friction at the interface provokes the rise of tangential stresses. The problem of determining tangential stresses within the contact area, in the partial-slip regime, was solved independently by Cattaneo (1938a,b,c) and Mindlin (1949). On the other hand, the complete solution for the stress field generated by a circular sliding contact is due to Hamilton and Goodman (1966). The principal stresses are both compressive in the contact region. If a yielding condition of failure is assumed (ductile materials), the authors concluded that the most likely region of failure is the front edge of the circle of contact. Only at the border of the circular contact area, radial tractions arise, accompanied by smaller circumferential compressions. In the case of brittle materials the appearance of tensile stresses is more important than the value of the yield parameter. These tensile stresses, whose value depends on the friction coefficient, give rise to the typical *ring cracks* at the edge of the contact zone, which constitute the initiation of the Hertzian fracture cones (see Section 1). Under usual conditions, tensile stresses attain their maximum value at the rear edge of the contact area.

Hanson (1993) determined the elastic field in the case of sliding conical punches. The stress fields induced by wedge and conical indenter have been extensively investigated also by Truman et al. (1995, 1996). As will be described in Section 4, the elastic stress fields beneath moving contact areas are commonly used to investigate the formation and propagation of cracks occurring in scratching and cutting processes.

3. Numerical investigation on the penetration process in heterogeneous materials

The elastic solutions described in the previous section are valid only in a small loading range. Due to damage and fracture, in fact, the indentation of quasi-brittle materials is strongly depending on the size and shape of the indenter and on the mechanical characteristics of the base material. Experimental studies by Pang et al. (1989) showed that, in general, plastic rocks are only crushed and penetrated by the indenter, giving linear curves, whereas more brittle rocks are cracked with the formation of chips, giving nonlinear and discontinuous curves. Both concave upward and concave downward curves can be obtained, and thus no unique statement can, in principle, be made.

In order to investigate the role of heterogeneity in quasi-brittle materials, numerical simulations of indentation by means of a *lattice model* (included in the FEM package DIANA^{TM}) have been carried out. The lattice model is a discrete model of a solid material where the continuum is replaced by an equivalent beam or truss structure, the *lattice*. The main purpose of the lattice model is to achieve understanding of the fracture processes which occur at small scales and of the influence of the microstructural disorder on the global behaviour of the material. A great advantage with respect to the classical codes based on fracture mechanics is that there is no need for an initial crack to be defined. Thereby, we do not need a positive stress-intensity factor K_I to ensure crack propagation, and the final macrocracks are naturally provided by the coalescence of the microcracks induced by disorder and heterogeneity inside the material.

The DIANA^{TM} lattice model is based on the algorithm proposed by Van Mier and co-workers (Van Mier, 1996) to simulate progressive failure in concrete. This model adopts beam elements rather than truss elements because local rotations at the nodes play a fundamental role in the fracture process, especially when

compressive stresses prevail and disordered materials are considered. The model is based on a regular triangular lattice where the heterogeneity of the material is modelled by means of a random distribution of the material properties of the beam elements in the lattice structure. The ratios between length, height and width of the beams are chosen in order to ensure a realistic overall response (e.g. elastic modulus and Poisson's coefficient) of the model.

Any statistical distribution or a mapping of a particle structure on the lattice mesh are possibilities of modelling the heterogeneity of the material. In our case, a three-phase granular material was generated according to a power-law size distribution and overlapped to the mesh (Fig. 11). The three phases respectively represent the hard particles (approximately 65% in volume), the matrix, and the interface transition zone, or bond zone. The lattice elements are linear elastic beams with different constitutive properties and different failure limits for each phase. The ratio among the tensile strengths σ_u of the three phases was chosen as:

$$\frac{\sigma_{u(\text{particles})}}{\sigma_{u(\text{matrix})}} = \frac{2}{1} \quad \text{and} \quad \frac{\sigma_{u(\text{bond})}}{\sigma_{u(\text{matrix})}} = \frac{1}{4}, \tag{13}$$

whereas the ratio among the elastic moduli was established as:

$$\frac{E_{(\text{particles})}}{E_{(\text{matrix})}} = \frac{3}{1} \quad \text{and} \quad \frac{E_{(\text{bond})}}{E_{(\text{matrix})}} = 1. \tag{14}$$

These ratios, which are representative of a wide class of rocks and are also close to normal structural concrete, clearly state the dominant role played by the weak interfaces in the damage process.

The lattice analysis is performed as a sequence of steps. Within every step, a linear elastic calculation is carried, and the force and moment distribution in the beam elements of the lattice structure are calculated. The maximum stress of the beam is used in the evaluation of a local *fracture law*. The standard fracture law, successfully tested in many situations (Van Mier, 1996), is given by:

$$\sigma = \frac{N}{A} + \beta \frac{\max(|M_{(i)}|, |M_{(j)}|)}{W} \geqslant \sigma_u, \tag{15}$$

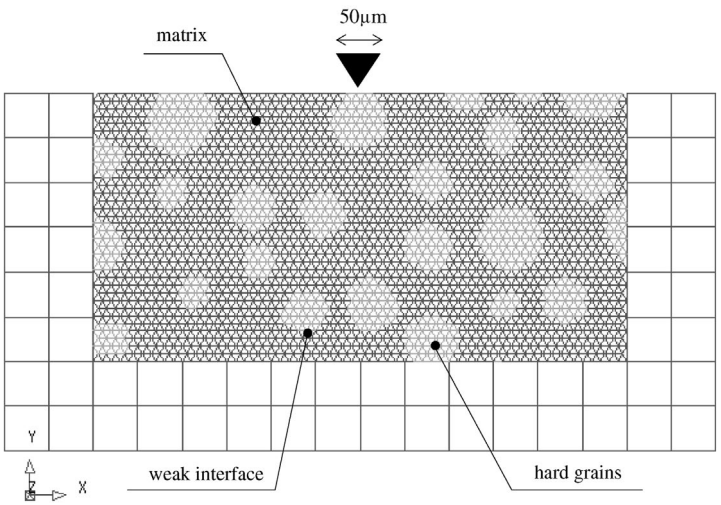

Fig. 11. Three-phase coarse material adopted in the lattice simulations ($l_{\text{beams}} = 5$ μm).

where $A = bh$ is the cross-sectional area of the beams and $W = (1/6)bh^2$ is the sectional modulus of the beams. The tensile strength σ_u is defined, for each phase, according to Eq. (13). The normal force N in each beam and the bending moments $M_{(i)}$ and $M_{(j)}$ in node i and node j respectively, are calculated during the linear elastic analysis of the structure. Crack growth and damage are simulated by removing elements from the lattice structure. At each step, the lattice element with the highest stress/strength ratio (according to Eq. (15)) is removed from the mesh, load is rescaled and a new step is performed, until the model becomes completely disconnected.

The parameter β in Eq. (15) is introduced to select a failure mode where bending plays either a dominant or a restricted role. When simulating tests where tensile stresses are predominant, the value of β can be set equal to 0.005–0.01 (Van Mier, 1996). On the other hand, this is not the case of indentation and cutting (especially in the presence of negative rake angles), because compressive fields are predominant and the role of local rotations becomes of major importance, as is well known in Cosserat elasticity. Therefore, in our simulations, β was optimized within the range $0.05 < \beta < 0.1$.

The action of a rigid indenter penetrating the lattice is modelled according to the scheme in Fig. 11. A displacement-controlled test is simulated, with rigid displacements assigned to the loaded nodes of the mesh. These displacements are calculated according to a conical shape of the indenter. A preliminary investigation on the role of the wedge angle 2α, in the range 90°–170°, has been carried out. It has been found that substantial differences are localized very close to the indenter (i.e. the stress–strain fields, of course, may considerably differ from the theoretical ones described in Section 2), whereas damage patterns are remarkably similar at a certain distance from the indenter.

Three different microstructures have been investigated:

(a) a *coarse microstructure*, with grain diameters ranging from 20 to 45 μm and well-defined ratios among the mechanical properties of the three phases (Eqs. (13) and (14));
(b) a *fine microstructure*, with grain diameters ranging from 10 to 20 μm, and with the same mechanical ratios of the previous case;
(c) an *almost homogeneous microstructure*, with the same granulometry of case (b), but with values of strength and stiffness of the three phases very close to each other ($\sigma_{u(particles)}/\sigma_{u(matrix)} = 1.10$, $\sigma_{u(bond)}/\sigma_{u(matrix)} = 0.95$, $E_{(particles)}/E_{(matrix)} = 1.3$, $E_{(bond)}/E_{(matrix)} = 1.0$).

Three different stages of the penetration process in the coarse microstructure are reported in Fig. 12, for the case of $2\alpha = 130°$ (notice that the deformations of the lattice beams are exaggerated in the graphic representation). Damage initially concentrates below the indenter, virtually forming a splitting crack (Fig. 12a). Contrarily to blunt indenters, the splitting cracks anticipate the formation of the cone cracks, which form only later (Fig. 12b). Finally, small fragments are detached along pseudo-horizontal lines (Fig. 12c). An index of damage Δ can be defined as the percentage of broken beams (N_{broken}) within the total number of lattice beams ($N_{tot} = 6341$ for this mesh).

The load-penetration diagram calculated for the coarse microstructure is shown in Fig. 13a. Notice that, after an initial nonlinear stage (which can be physically ascribed to surface effects occurring at microscales), the behaviour is practically linear, as predicted by the experiments (Cook et al., 1984). The local *snap backs* in the diagram, which cannot be captured by the experimental tests, show the intrinsic local brittleness of the phases, which is hindered by material heterogeneity. In the case of the finer particle distribution, the trends are practically the same, except for a more compliant behaviour (Fig. 13b). Instead, when simulating indentation in an almost homogeneous lattice, a more brittle behaviour was obtained. Damage did not spread in the bulk, but was concentrated in a narrow splitting band.

It can be concluded that heterogeneity and microcracking imply a totally different load-penetration response with respect to the elastic predictions. A downward concavity is present, i.e., the compliance to indentation increases with load. The curves can be consistently discretized by a bilinear relation (Fig. 13).

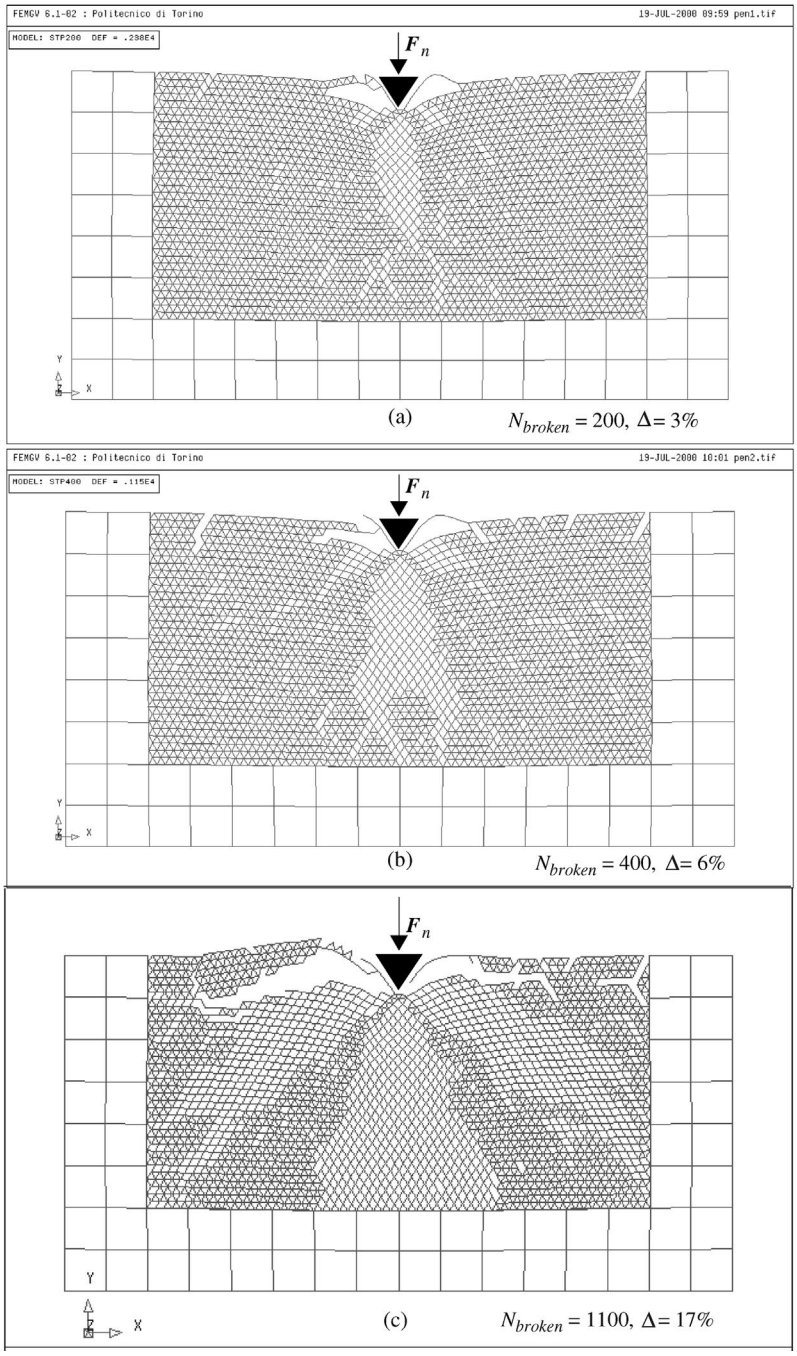

Fig. 12. Evolution of damage in the lattice mesh (coarse material) with increasing the indentation load F_n.

However, for the purpose of simple modelizations, we can consider the first stage as a transient stage. Indeed, it is well known that below a threshold value of F_n only *polishing* of the surface occurs, and efficient

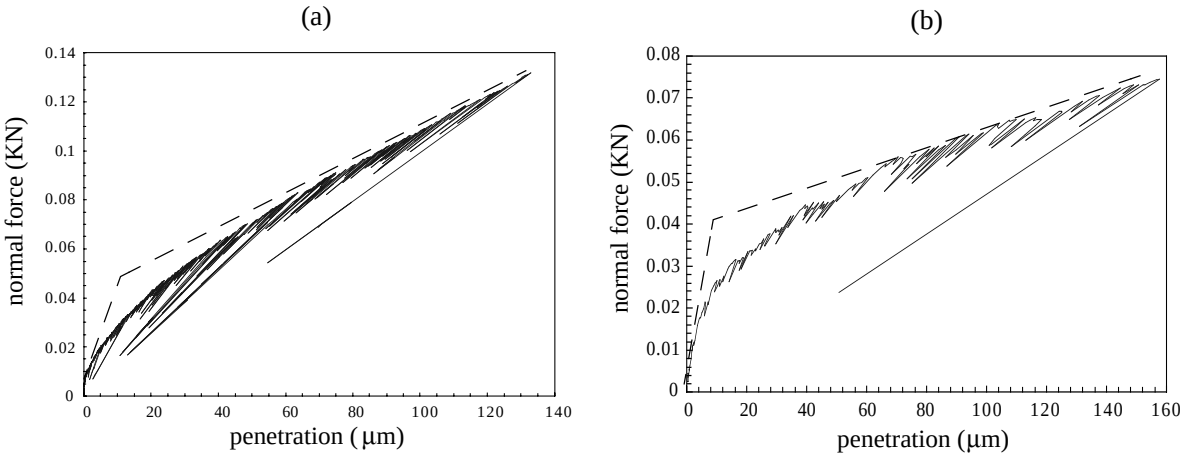

Fig. 13. Numerical load-penetration diagrams for the (a) coarse and the (b) fine microstructures. Notice that the curves are well approximated by a bilinear relation.

cutting does not take place. Thus, in the case of quasi-brittle materials, a linear relation ($F_n = kw$) can be adopted, with good approximation, in the stationary cutting regime.

4. Models for the scratching and cutting actions of indenters

As already mentioned in the introduction, the mechanics governing the process of cutting quasi-brittle materials has not been adequately investigated, especially if compared to the classical studies on metal cutting (Merchant, 1944). In the case of very brittle materials like glass, some researchers tried to apply the concepts of LEFM to the crack propagation under sliding contacts, with and without friction (Conway and Kirchner, 1980; Chiang and Evans, 1983; Mouginot and Maugis, 1985; Chen et al., 1991).

Lawn (1967) developed a fracture mechanics theory for the propagation of pre-existing mono-dimensional flaws in brittle materials under the hypothesis of full-slip interfacial conditions. Conway and Kirchner (1980) investigated the mechanics of crack initiation and propagation beneath a moving sharp indenter. The Mitchell solution was adopted for the determination of stress distributions below the indenter for selected horizontal/vertical load ratios. A fracture mechanics solution for embedded penny-shaped cracks was used to predict the propagation depth of pre-existing defects. It was found that the radial tensile stresses behind the tool justify the U-shaped cracks in the track (see Fig. 9), whereas chipping ahead of the tool could not be modelled. Chiang and Evans (1983) considered the propagation of semi-circular pre-existing cracks in ceramics, under partial-slip conditions. The fracture initiation load was predicted to depend sensitively on the magnitude of the applied tangential force F_t and on the interfacial friction coefficient. Similar investigations were carried out by Chen et al. (1991), by Keer and Kuo (1992), who found a linear relation between applied load and the extent of damage, and by Shah and Long (1997) in the case of quasi-brittle rocks.

Bower and Fleck (1994) adopted a boundary element technique to investigated the propagation of cracks under a two-dimensional Hertzian contact sliding over a half-space containing several microcracks. It was shown that only extremely brittle materials are likely to fail by brittle fracture. In other materials failure should depend on the combination of plastic flow and fracture. A periodic array of cracks forms in the wake of the slider, but the condition of formation of a chip were not found. It could only be stated that the

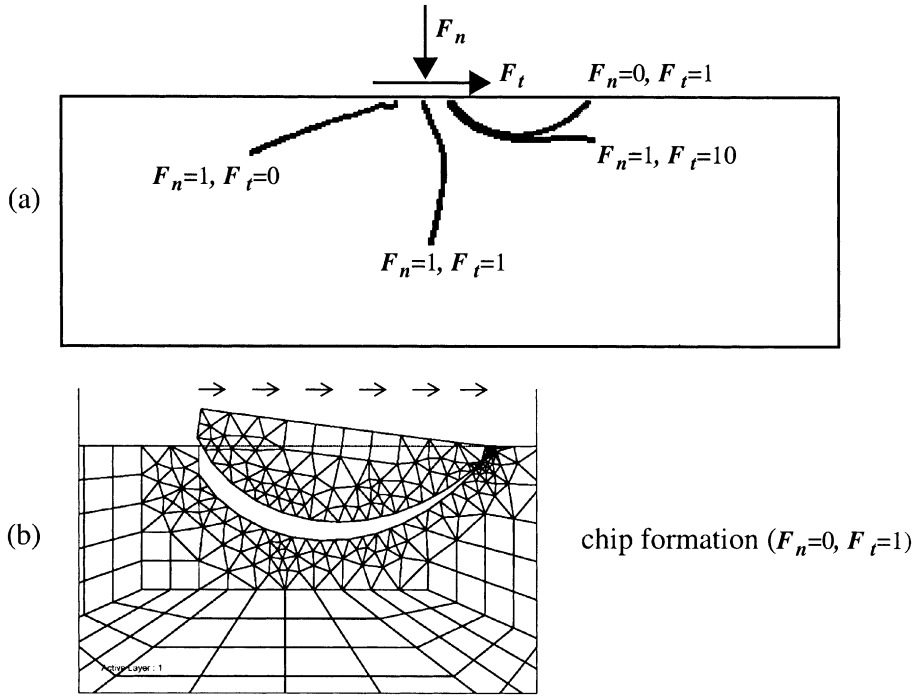

Fig. 14. Finite elements simulations of brittle cracking under a sliding indenter. Role of the tangential force.

size of the (potential) fragment increases with increasing the ratio between the normal and the tangential force (F_n/F_t). The primary role of the tangential forces acting on the interface has been verified also by finite elements analyses (Invernizzi, 2000) of Mode I crack propagation. In Fig. 14a, one can recognize the classical Hertzian cone cracks developing when only normal loading is present, or the pseudo-vertical splitting cracks generated by equal values of normal and tangential loading. The case where only tangential tractions are present corresponds to the chip formation depicted in Fig. 14b, whereas the intermediate case ($F_t/F_n = 10$) yields horizontal crack propagation.

All the aforementioned authors considered a sliding contact area, without taking into account real penetration. Thus, their approaches are limited to surface scratching. Moreover, they commonly assumed the existence of pre-existing flaws inside the base material, and followed their propagation under the induced elastic stress fields. However, even in the simplest configurations, it is very awkward to make predictions on the size of the chips and on the force on the tool. Although many of these studies are remarkable, their applicability to materials exhibiting damage and plasticity in a finite process zone is, at least, questionable.

On the other hand, most of the work on the cuttability of rocks and concrete is based on either specific local experiments or on empirical rating systems. No general method exists for predicting the forces acting on a cutting tool, based only on material properties and machine parameters. Among the few attempts to evaluate the cutting force on physical bases, it is worth to mention Mishnaevsky (1994), who investigated the real cutting process in brittle materials, considering the role of different physical mechanisms involved in material destruction (deformation, crushing, cracking and spalling). He found that neither Hertzian cone cracks nor circumferential cracks are formed. Instead, penny-shaped cracks, lying in a plane containing the cutting force vector, are formed. He also derived a pseudo-empirical formula for the cutting force and for

the depth of the damaged zone, but the determination of the material parameters involved in the formulas is clumsy. In Mishnaevsky (1995), the process of rock fragmentation is described, and the destructive role of the stress field inhomogeneity is discussed.

A recent approach by Alehossein and Hood (1999) is based on the application of dimensional analysis to cutting experiments. Starting from eight independent parameters, the problem is reduced to only five independent group variables, whose exponents can be determined by least-squares regression. The outcome is a linear arrangement of the experimental data which permits to obtain reliable predictions of the cutting force in real situations.

The action of a ploughing indenter can be simulated by the lattice model by prescribing vertical and horizontal rigid displacements to the loaded nodes. In Fig. 15 three different stages are reported, for the case of the coarse microstructure, where $F_t \approx F_n$. Since the cutting force is equal to the normal force, tensile stresses prevail behind the indenter, while a strong compressive field arises ahead of it. As suggested by the elastic stress field, cracks initially develop *behind* the indenter (Fig. 15a), in the form of vertical splitting fractures. Only when the material becomes significantly weakened in this zone, damage begins to spread inside the compressive field (Fig. 15b). However, due to the tension-governed fracture law, the lattice model cannot predict fragmentation within the compressed zone, and only surface delamination is observed in the last stages (Fig. 15c). Notice, however, the large amount of broken beams (due to the local splitting mechanism in the lattice network) along the maximum compression diagonal direction.

Recalling the FEM results reported in Fig. 14, it can be affirmed that not only when sliding contacts are considered, but also in a real scratching process, crack patterns strongly depend on the ratio F_t/F_n. In cutting experiments (Lopez Jimeno et al., 1995; Mishnaevsky, 1994, 1995), it is well known that, as the penetration w increases, the ratio F_t/F_n increases too, and thus vertical splitting cracks leave place to pseudo-horizontal fractures. Of course, the size of the fragments depends on the penetration (it is plausible that it increases with F_n), and thus it is crucial to estimate some kind of relation between penetration, normal force and cutting force.

In order to find general relations between the value of the cutting force F_t and that of the normal force F_n, in the following three different physical mechanisms of material removal are examined, namely a simple frictional mechanism, plastic crushing and LEFM. In the real situations, the mechanisms interact in a manner depending on the material characteristics and other parameters (e.g., shape of the indenter, applied strain rate etc.). For instance, the width of the cutting tool may have substantial effects on the state of stress in front of the tool, providing deviations from the theoretical assumptions, due to three-dimensional effects. Therefore, the models should be adequately combined, in the real cases, to estimate the correct value of the cutting force. However, since the following relations come from very general dimensional arguments, they represent limit cases which cannot be exceeded.

The starting point is the definition of the load-penetration law. In the most general case, we could consider a relation like $F_n = kw^\lambda$, where $\lambda > 1$ implies upward concavity of the law, $0 < \lambda < 1$ implies downward concavity, and $\lambda < 0$ implies negative slope, e.g. softening regimes for very high loading ranges. In the case of plastic rocks, the indentation experiments would suggest a slight downward concavity ($\lambda < 1$). On the contrary, in the presence of hard rocks with high yield limit, it is more consistent to chose an upward concavity ($1 < \lambda < 2$). However, as already stated before, experimental tests (Cook et al., 1984; Pang et al., 1989) allow us to adopt, in many cases, a linear dependence ($\lambda = 1$) between the normal force F_n acting upon the indenter and its penetration w, at least below a certain loading value. The lattice model analyses (see Section 3) confirmed this assumption, if the polishing stage is disregarded.

The simplest model considers the cutting force to be directly proportional to the normal force acting upon the indenter. This corresponds to treat all the dissipation occurring during material removal as a frictional process, i.e. to adopt a linear Coulomb's law:

$$F_t = \mu F_n. \tag{16}$$

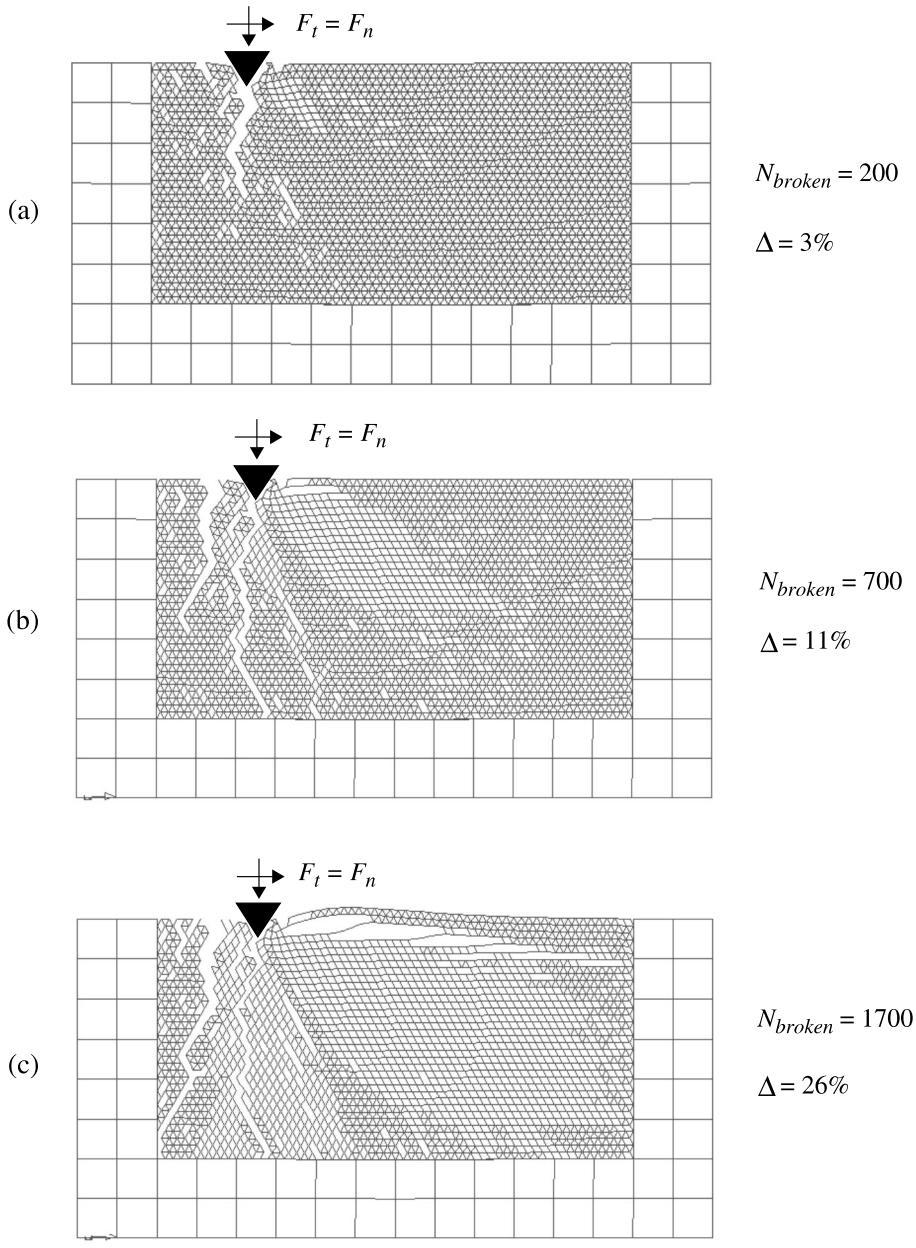

Fig. 15. Lattice simulation of the ploughing action of a rigid indenter in a heterogeneous material.

The parameter characterizing material behaviour, in this case, is the friction coefficient μ. This is the assumption currently adopted in most of the models in the literature, i.e. that of a contact area sliding with friction upon a half-space. Although its simplicity, the real situation is totally different, because the indenter penetrates inside the material. Moreover, it is very unrealistic to include all the dissipations (crushing, chipping) in a friction coefficient.

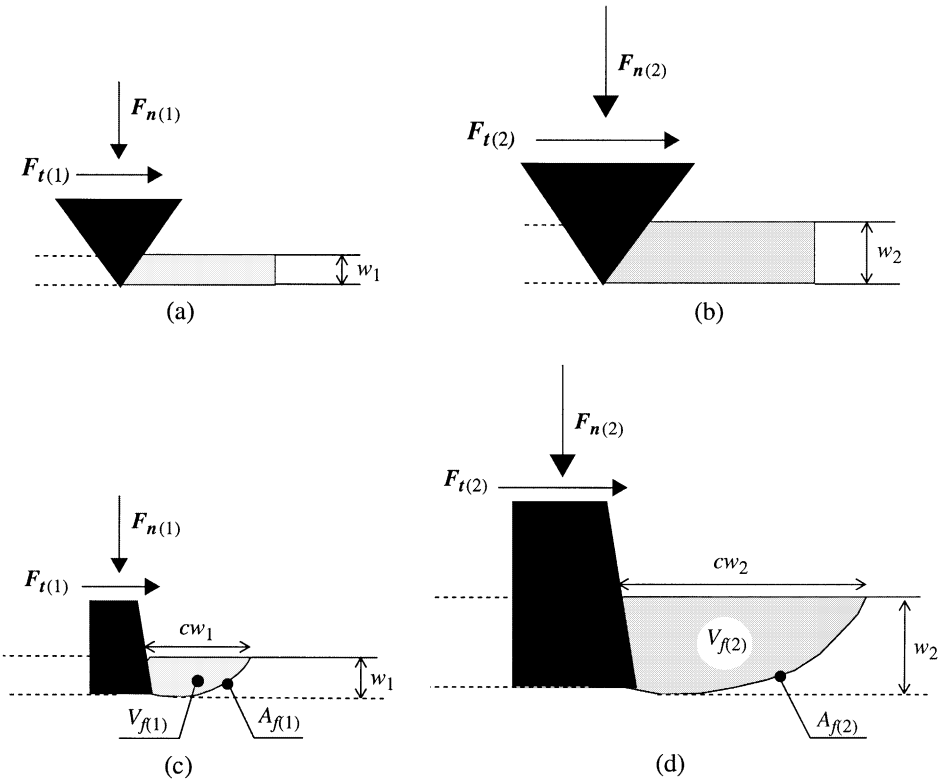

Fig. 16. Geometrical similitude in the (a,b) continuous plastic crushing process, and in the (c,d) discontinuous brittle chipping process.

A more realistic model considers a continuous crushing action of the indenter, and assumes a strength criterion for material collapse. In this case, the cutting force must depend on a different material parameter, namely the *cutting strength* S, which can be alternatively intended as the crushing strength of the base material ($S = [F][L]^{-2}$), or as the specific energy necessary to remove the unit volume ($S = [J][L]^{-3}$), i.e., the *specific cutting energy*. Since the cross-section of the continuous chip (Fig. 16a and b) is the controlling parameter, dimensional analysis implies that the cutting force must depend on the square of the penetration:

$$F_t = S\gamma w^2, \tag{17}$$

where γ is a non-dimensional factor depending on the shape of the groove. By inserting the general power law form of the penetration law ($F_n = kw^\lambda$), one obtains:

$$F_t = S\gamma \frac{F_n^{2/\lambda}}{k^{2/\lambda}}, \tag{18}$$

which can be specialized, respectively for the case of linear ($\lambda = 1$) and quadratic ($\lambda = 2$) penetration laws, as:

$$F_t = S\gamma \frac{F_n^2}{k^2}, \tag{19a}$$

$$F_t = S\gamma \frac{F_n}{k}. \tag{19b}$$

Notice, of course, that the physical dimensions of the material stiffness k depend on the exponent λ of the penetration law.

The third model considers discontinuous chipping and is based on LEFM (Fig. 16c and d). If a brittle fracture criterion is adopted for material collapse, the fracture toughness K_{IC} becomes the material parameter to be considered ($K_{IC} = [F][L]^{-3/2}$). Dimensional analysis, in this case, provides:

$$F_t = K_{IC}\chi w^{3/2}, \tag{20}$$

where χ is a non-dimensional shape factor. Inserting the general form of the penetration law, one obtains:

$$F_t = \chi \frac{K_{IC}}{k^{3/2\lambda}} F_n^{3/2\lambda}. \tag{21}$$

which yields, respectively in the case of linear and quadratic penetration laws:

$$F_t = \gamma \frac{K_{IC}}{k^{3/2}} F_n^{3/2}, \tag{22a}$$

$$F_t = \gamma \frac{K_{IC}}{k^{3/4}} F_n^{3/4}. \tag{22b}$$

Notice that, whatever the penetration law, the dependence of F_t on F_n is less pronounced in the case of brittle chipping than in the case of plastic crushing. Given the same penetration in the material, equal cutting velocities can be obtained with less effort. Therefore, it is natural to conclude that chipping represents a more efficient way of cutting materials, with respect to crushing. Optimization of cutting tools can, in principle, be pursued by enhancing the chipping ability of the indenter (e.g., by proper shaping of the tool, positive rake angles, etc.). Very localized actions (e.g., high stress singularities) also enhance the chipping ability (Mishnaevsky, 1995).

5. Size effects induced by brittle chipping on cutting strength

The simple discontinuous chipping model for cutting provides very interesting results regarding the scaling laws involved in the phenomenon. Let us consider two different indenters, pushed inside the base material by different values of the normal force (Fig. 16c and d). Of course, two different values of the cutting force F_t are induced by the two different situations. It is physically plausible to assert that *self-similarity* holds in the distribution of the fragments removed by the ploughing indenters. The similitude is supported by the fractal power-law distributions obtained by many fragmentation and cutting experiments (see the extensive collection of data by Turcotte (1992)). Thereby, assuming the penetration w as the reference length scale, the volume V_f of the removed chip scales as w^3, while the area of the fracture surface A_f scales as w^2.

As is customary in the cutting and drilling practice, the mechanical parameter which defines the material resistance is the cutting strength S which, in the framework of plasticity, has to be considered a scale-independent parameter (see Eq. (17)). Indeed, the cutting process is discontinuous (see Figs. 8 and 9). Thereby, removal of the fragment is governed by LEFM, and the cutting strength undergoes relevant size effects.

According to LEFM, the failure criterion must be written in terms of the stress-intensity factor K_I (with physical dimensions $[F][L]^{-3/2}$), to be compared with the fracture toughness of the material K_{IC}. Thus, the cutting force F_t has to obey the following relation:

$$K_I = \frac{F_t}{\chi w^{3/2}} f(x, y, z) = K_{IC}, \tag{23}$$

where χ is a non-dimensional geometrical factor and $f(x,y,z)$ is a non-dimensional geometrical function. Dimensional analysis yields, in this case, the following scale dependence of the cutting force on the penetration: $F_t \sim w^{3/2}$. The above scaling law can also be justified by the dimensional disparity inherent to the energy balance. The elastic strain energy stored in the fragment, in fact, scales as w^3, whereas the energy which can be dissipated along the fracture surface scales as w^2. In the case of plastic crushing, instead, both energies would scale as w^3. The intrinsic nonlinearity of chipping (which is independent of the penetration law) implies that a Coulomb-like linear relation is misleading. In fact, in typical cutting experiments (Mishnaevsky, 1994, 1995), the ratio F_t/F_n increases with w.

Due to geometrical self-similarity of chips, one can assert that the work W done by the cutting force when removing a single fragment is given by the product of the force times a displacement cw (Fig. 16b and c). Therefore, recalling Eq. (23):

$$W_{\text{cutting}} = (F_t cw) \sim w^{5/2}, \tag{24}$$

where c is a non-dimensional geometrical factor. By definition, the specific work per unit volume is the *cutting strength* S, with physical dimensions $[J][L]^{-3}$. From Eq. (24) one obtains the following scaling law for the cutting strength:

$$S = \frac{W_{\text{cutting}}}{\kappa w^3} \sim \frac{1}{\sqrt{w}}, \tag{25}$$

where κ is a non-dimensional geometrical factor. The scaling law (25), depicted in Fig. 17, is very interesting and is confirmed by the experiments (see, for instance, the experimental decrease of strength shown in Fig. 7). Therefore, if brittle chipping is the main destructive mechanism, the nominal cutting strength S decreases with the penetration w or, which is equivalent, with the size of the indenter. Bigger indenters will therefore be more efficient cutters, although a larger normal force will be necessary to ensure their penetration. These considerations should be taken in adequate account when performing cutting and drilling operations. Incidentally, it is well known, in the drilling practice, that larger chip sizes imply a better efficiency (i.e. less energy expenditure). As already mentioned before, the square root scaling should be modified in real situations, because a certain extent of crushing always occurs immediately ahead of the indenter, and thus the two destruction mechanisms interact with each other (Van Kesteren, 1995). In particular, plastic crushing can be very important in some kinds of rocks and even prevail over brittle fracture. Moreover, dynamic effects related to high strain rates can also alter the theoretical predictions.

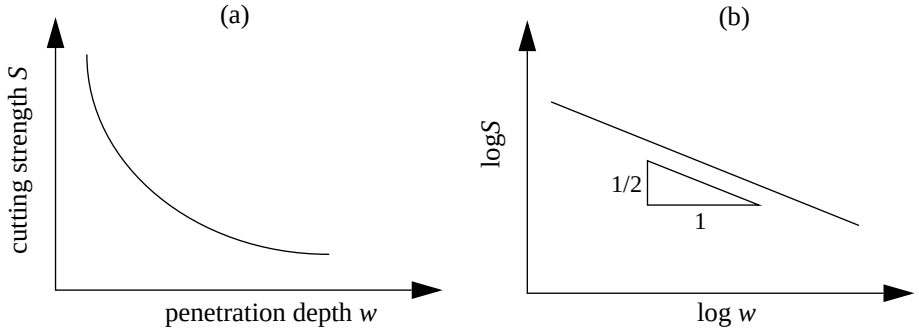

Fig. 17. Size-effects on the cutting strength S according to (a) LEFM; (b) bi-logarithmic diagram.

6. Conclusions

In this paper, after an overview of the existing approaches to the problem, some general relations valid for the cutting process in brittle and quasi-brittle materials have been put forward. With the help of numerical simulations by the lattice model, the roles of material heterogeneity and damage have been investigated. It has been shown that various mechanisms interact ahead of the indenter during the cutting process, and mainly plastic crushing and brittle chipping. Since the process is discontinuous, some characteristic lengths of damage come into play, related to the indenter's penetration, which provide size effects on the cutting strength of the material. Thereby, it was concluded that the cutting performances can be significantly improved by reducing the crushing component and enhancing the chipping ability of the indenters. In the context of cutting tools design, increasing the size of the indenters improves the local fracture mechanisms but also implies the necessity for larger normal forces and for higher energy supply. Thus, the practical situations require the optimal combination between machine power, base material resistance and cutting ability of the tool. Classical approaches consider S as a material's constant, which is not the case, as shown in the paper. Larger indenters (or deeper penetration depths) behave more effectively than smaller ones, because the energy expenditure is considerably smaller for a given volume of removed material.

Acknowledgements

Support by the Italian Ministry of University and Research (MURST) and by the National Research Council (CNR) is gratefully acknowledged by the author.

References

Alehossein, H., Hood, M., 1999. An application of linearized dimensional analysis to rock cutting. Int. J. Rock Mech. Min. Sci. 36, 701–709.

Barber, J.R., 1992. Elasticity. Kluwer, Dordrecht.

Borri-Brunetto, M., 2000, private communication.

Bower, A.F., Fleck, N.A., 1994. Brittle fracture under a sliding line contact. J. Mech. Phys. Solids 42, 1375–1396.

Carpinteri, A., 1989. Decrease of apparent tensile and bending strength with specimen size: two different explanations based on fracture mechanics. Int. J. Solids Struct. 25, 407–429.

Cattaneo, C., 1938a. Sul contatto di due corpi elastici: distribuzione locale degli sforzi. Rendiconti dell'Accademia Nazionale dei Lincei 27, 342–348.

Cattaneo, C., 1938b. Sul contatto di due corpi elastici: distribuzione locale degli sforzi. Rendiconti dell'Accademia Nazionale dei Lincei 27, 434–436.

Cattaneo, C., 1938c. Sul contatto di due corpi elastici: distribuzione locale degli sforzi. Rendiconti dell'Accademia Nazionale dei Lincei 27, 474–478.

Chen, S.Y., Farris, T.N., Chandrasekar, S., 1991. Sliding microindentation fracture of brittle materials. Tribol. Trans. 34, 161–168.

Chiang, S.S., Evans, A.G., 1983. Influence of a tangential force on the fracture of two contacting elastic bodies. J. Am. Cer. Soc. 66, 4–10.

Conway, J.C., Kirchner, H.P., 1980. The mechanics of crack initiation and propagation beneath a moving sharp indentor. J. Mat. Sci. 15, 2879–2883.

Cook, N.G.W., Hood, M., Tsai, F., 1984. Observations of crack growth in hard rock loaded by an indenter. Int. J. Rock Mech. Min. Sci. 21, 97–107.

Cook, R.F., Pharr, G.M., 1990. Direct observation and analysis of indentation cracking in glasses and ceramics. J. Am. Cer. Soc. 73, 787–817.

Hamilton, G.M., Goodman, L.E., 1966. The stress field created by a circular sliding contact. J. Appl. Mech. 33, 371–376.

Hanson, M.T., 1993. The elastic field for a sliding conical punch on an isotropic half-space. J. Appl. Mech. 60, 557–559.

Hertz, H., 1882. Über die Berührung fester elastischer Körper. J. Reine und Angewandte Mathematik 92, 156–171.

Hill, R., 1950. Mathematical Theory of Plasticity. Clarendon Press, Oxford.
Hills, D.A., Nowell, D., Sackfield, A., 1993. Mechanics of Elastic Contacts. Butterworth-Heinemann, Oxford.
Invernizzi, S., 2000, private communication.
Johnson, K.L., 1985. Contact Mechanics. Cambridge University Press, Cambridge.
Keer, L.M., Kuo, C.H., 1992. Cracking in a loaded, brittle elastic half-space. Int. J. Solids Struct. 29, 1826–1829.
Lawn, B.R., 1967. Partial cone crack formation in a brittle material loaded by a sliding spherical indenter. Proc. R. Soc. London A 299, 307–320.
Lawn, B.R., Wilshaw, R., 1975. Indentation fracture: principles and applications. J. Mat. Sci. 10, 1049–1081.
Lawn, B.R., Swain, M.V., 1975. Microfracture beneath point indentations in brittle solids. J. Mat. Sci. 10, 113–122.
Lopez Jimeno, C., Lopez Jimeno, E., Ayala Carcedo, F., 1995. Drilling and Blasting of Rocks. Balkema, Rotterdam.
Love, A.E.H., 1939. Boussinesq's problem for a rigid cone. Quart. J. Math. 10, 161–175.
Merchant, M.E., 1944. Basic mechanics of the metal cutting process. J. Appl. Mech. Trans. ASME 66, 168–186.
Mindlin, R.D., 1949. Compliance of elastic bodies in contact. J. Appl. Mech. 16, 259–268.
Mishnaevsky, L.L., 1994. Investigation of the cutting of brittle materials. Int. J. Mach. Tools Manuf. 34, 499–505.
Mishnaevsky, L.L., 1995. Physical mechanisms of hard rock fragmentation under mechanical loading: a review. Int. J. Rock Mech. Min. Sci. 32, 763–766.
Mouginot, R., Maugis, D., 1985. Fracture indentation beneath flat and spherical punches. J. Mater. Sci. 20, 4354–4376.
Pang, S.S., Goldsmith, W., Hood, M., 1989. A force-indentation model for brittle rocks. Rock Mech. Rock Engng. 22, 127–148.
Roesler, F.C., 1955. Indentation hardness of glass as an energy scaling law. Proc. Phys. Soc. London 58, 55–60.
Shah, K.R., Long, T.F., 1997. Fracturing at contact surfaces subjected to normal and tangential loads. Int. J. Rock Mech. Min. Sci. 34, 727–739.
Sneddon, I.N., 1965. The relation between load and penetration in the axisymmetric Boussinesq problem for a punch of arbitrary profile. Int. J. Engng. Sci. 3, 47–57.
Truman, C.E., Sackfield, A., Hills, D.A., 1995. Contact mechanics of wedge and cone indenters. Int. J. Mech. Sci. 37, 261–275.
Truman, C.E., Sackfield, A., Hills, D.A., 1996. The state of stress induced by a conical indenter. J. Strain Anal. 31, 325–327.
Turcotte, D.L., 1992. Fractals and Chaos in Geology and Geophysics. Cambridge University Press, Cambridge.
Van Kesteren, W.G.M., 1995. Numerical simulations of crack bifurcation in the chip forming cutting process in rock. In: Baler, G., Karihaloo, B.L. (Eds.), Fracture of Brittle Disordered Materials. E & FN Spon, London, pp. 505–524.
Van Mier, J.G.M., 1996. Fracture Processes of Concrete. Assessment of Material Parameters for Fracture Models. CRC Press, Boca Raton.